Pandora's Lattice: Family-Synchronized States in a Globally Coupled Logistic Map Lattice

Andrew R. Jacobson

1 Introduction

The system of interest in this study is a lattice of N globally coupled one dimensional maps. The lattice evolution is described by

$$x_{n+1}(i) = (1-\epsilon)f[x_n(i)] + \frac{\epsilon}{N}\sum_{j=1}^{N} f[x_n(j)], \tag{1}$$

where i and j are indices of maps within the lattice, n and $n+1$ are iteration indices, the coupling strength is ϵ, and $f(x)$ is the map function. $x_n(i)$ is the nth iteration of the ith map in the lattice. The coupling strength ϵ varies between zero and one.

All the lattices discussed in this study are constructed using logistic maps of the form

$$f(x_n) = 1 - ax_n^2. \tag{2}$$

For reference, a bifurcation diagram for this form of the logistic map is shown in Figure 1. This map has the property that any condition on the interval [-1 1] will remain on that interval under iteration of the map.

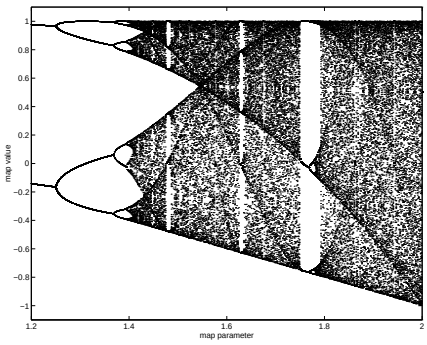

Figure 1: Logistic map bifurcation diagram.

We should especially note that since the coupling term is constructed of equal contributions from each map in the lattice, there is no spatial dependence in this system.

2 Strong Coupling Limit

As the coupling strength approaches unity, we expect the lattice to tend to a fully-synchronized state. In this limit, all the maps take on the same value and follow the same evolution, which is that of a single, uncoupled logistic map.

There is a threshold coupling value for the lattice above which the system will synchronize. This critical coupling value, ϵ_c, may be computed using linear stability analysis. To do so, we rewrite the N-dimensional lattice evolution (1) in matrix form as $\mathbf{x}_{n+1} = \mathbf{C}\,\mathbf{f}(\mathbf{x}_n)$, where the coupling matrix $\mathbf{C}$ is given by

$$\mathbf{C} = \begin{pmatrix} 1-\epsilon+\frac{\epsilon}{N} & \frac{\epsilon}{N} & \frac{\epsilon}{N} & \cdots & \frac{\epsilon}{N} \\ \frac{\epsilon}{N} & 1-\epsilon+\frac{\epsilon}{N} & \frac{\epsilon}{N} & \cdots & \frac{\epsilon}{N} \\ \vdots & \vdots & \vdots & \vdots & \vdots \\ \frac{\epsilon}{N} & \frac{\epsilon}{N} & \frac{\epsilon}{N} & \cdots & 1-\epsilon+\frac{\epsilon}{N} \end{pmatrix}, \tag{3}$$

and

$$\mathbf{f}(\mathbf{x}_n) = \begin{pmatrix} f[x_n(1)] \\ f[x_n(2)] \\ \vdots \\ f[x_n(N)] \end{pmatrix}.$$

The coupling matrix C may also be written as $(1-\epsilon)\mathbf{I}_N + \frac{\epsilon}{N}\mathbf{1}_N$, where $\mathbf{I}_N$ is the $N \times N$ identity and $\mathbf{1}_N$ is an $N \times N$ matrix of all ones.

The Jacobian matrix at iteration n is $\mathbf{J}_n = \mathbf{C}\,\mathbf{F}'(\mathbf{x}_n)$, with

$$\mathbf{F}'(\mathbf{x}_n) = \begin{pmatrix} f'[x_n(1)] & f'[x_n(1)] & \cdots & f'[x_n(1)] \\ f'[x_n(2)] & f'[x_n(2)] & \cdots & f'[x_n(2)] \\ \vdots & \vdots & \vdots & \vdots \\ f'[x_n(N)] & f'[x_n(N)] & \cdots & f'[x_n(N)] \end{pmatrix}.$$

A small perturbation $\delta\mathbf{x}$ to the synchronized state $x_i = x$ therefore evolves according to

$$\begin{pmatrix} \delta x_{n+1}(1) \\ \delta x_{n+1}(2) \\ \vdots \\ \delta x_{n+1}(N) \end{pmatrix} = \mathbf{J}_n \begin{pmatrix} \delta x_n(1) \\ \delta x_n(2) \\ \vdots \\ \delta x_n(N) \end{pmatrix}. \tag{4}$$

The leading eigenvector of the Jacobian matrix lies entirely within the synchonization manifold and represents the evolution of the manifold itself. The Lyapunov exponent corresponding to this mode, λ_1, is that of the uncoupled logistic map. As reported by Kaneko [Kaneko, 1990] and Ding and Yang [Ding and Yang, 1997], the remaining $N-1$ eigenvectors

represent growth transverse to the manifold. Their Lyapunov exponents are degenerate and related to the exponent of the uncoupled map: $\lambda_2 = \lambda_3 = \cdots = \lambda_1 + \ln(1+\epsilon)$.

This leads to a simple criterion for the appearance of full synchronization within the system. For the synchronization manifold to be attracting, we require that $\lambda_1 + \ln(1+\epsilon)$ have an absolute value less than unity. In chaotic regions of the logistic map, $\lambda_1 > 1$, and the value of the critical coupling strength is

$$\epsilon_c = 1 - e^{\lambda_1}. \tag{5}$$

3 Existence of Other Global Attractors

One application of globally coupled map lattices that is frequently mentioned is to arrays of Josephson junctions. In 1989, Weisenfeld and Hadley [Weisenfeld and Hadley, 1989] published a paper in which they report on a mutiplicity of coexistent stable solutions in coupled arrays of Josephson junctions. They found a large number (order of $(N-1)!$) of stable limit cycles within such a system, and remarked on how small white noise perturbations may induce the system to jump from one basin of attraction to another. They called this phenomenon "attractor crowding", and showed that it may also be found in a system of coupled circle maps.

Shortly thereafter, Kaneko [Kaneko, 1989, Kaneko, 1990] reported finding similar results in a globally coupled logistic map lattice. In addition, he found a rich variety of "family"-synchronized solutions. These stable solutions are global attractors for which the N maps are partitioned into k groups with N_k members each. Each of these groups is a "family", and within each family, all the maps are synchronized to one another. The term "clustering" has been used in the literature to describe these types of solutions. We wish to avoid the connotation of spatial proximity associated with this term, however.

An example of such an attractor in which the lattice falls into a two family attractor is depicted in Fig. 2. The 100 maps are partitioned unequally into the two families; the larger family has 91 members and the smaller has 9 members. Note also that as expected, the members of the smaller family are located haphazardly within the lattice. This is solely a result of the randomly chosen initial conditions.

3.1 Coexistent Global Attractors

One of the interesting features of the system (1) is that there can be mutiple global attractors coexisting at the same parameter values (Fig. 3). In practice, a lattice falls into one basin of attraction or another depending on the initial values of the maps. There is evidence that some of the basins of attraction fill a considerable portion of phase space. At $a = 1.9$ and for coupling strengths of around $\epsilon = 0.385$, we find that randomly-initialized lattices fall robustly into one of three categories of two-family attractors: (i) $N_1 = 90$, $N_2 = 10$, period 3, (ii) $N_1 = 91$, $N_2 = 9$, period 3, (iii) $N_1 = 92$, $N_2 = 8$, chaotic. The attractor of Fig. 2 is of type (ii), and the attractor of Fig. 3 is of type (iii). The third return map of the chaotic attractor (Fig. 3, left panel) has an apparently fractal nature reminiscent of that of the Hénon map; as the figure is succesively enlarged, more and more lines become evident.

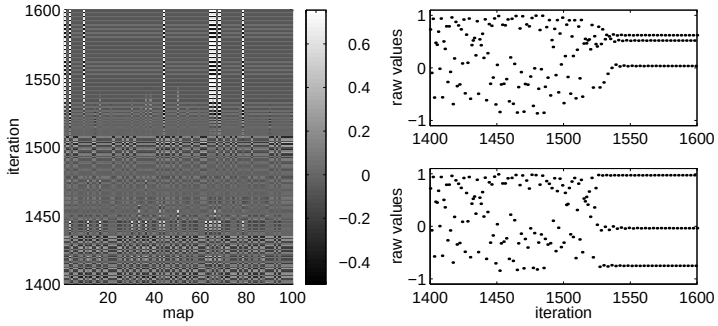

Figure 2: Transition to a two-family attractor for the globally coupled logistic map lattice at map parameter value a=1.9, lattice size N=100 and coupling strength $\epsilon = 0.385$. The maps of the lattice were initialized with random values. In this attractor, the larger family has 91 members, and the smaller family has 9. (left) Lattice-iteration diagram showing map values as a function of iteration before and after transition to the global attractor. To show contrast between families, the lattice mean at each iteration has been removed. (right, top) Time series of raw map values for map 1, which becomes a member of the smaller family. (right, bottom) Time series for map 2, a member of the larger family.

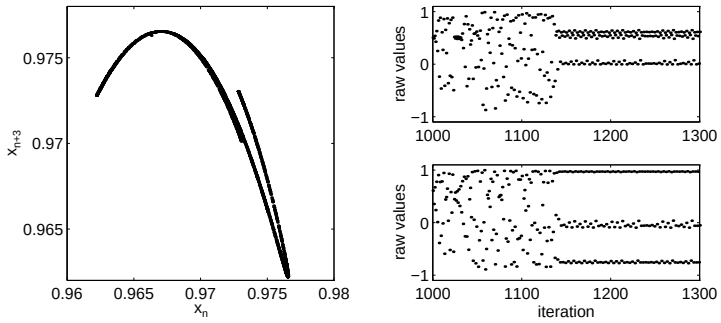

Figure 3: A second two-family attractor for a map lattice identical to that of Fig. 2. This attractor is chaotic. The larger family has 92 members, and the smaller family has 8. (left) Third return map for larger family. (right,top) Time series of raw map values for map #1, which becomes a member of the smaller family. (right, bottom) Time series for map #2, a member of the larger family.

4 Phase diagram

One of the prinicipal results of this summer's work is a refinement of the "phase portrait" presented by Kaneko [Kaneko, 1989, Kaneko, 1990]. This new diagram (Fig. 4) was created with 50 randomly initialized runs at each of 1570 points in the map parameter-coupling strength

plane. The map parameter a was varied between 1.4 and 1.98 in steps of 0.02; the coupling strength ϵ was varied from 0.1 to 0.5 in steps of 0.075. There is a rectangular window at $\epsilon > 0.3$ and $a < 1.42$ for which results were not computed.

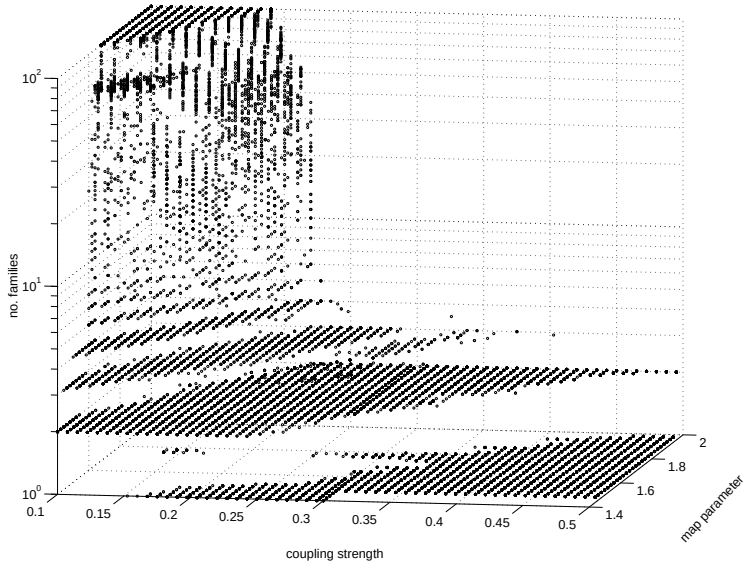

Figure 4: Number of families in statistically-stationary final states as a function of coupling strength ϵ and map parameter a. A dot at a given point means that some number of the runs at the corresponding a and ϵ values had final states with that number of families. Note that the vertical axis is logarithmic. Methodology is described in the text.

For each run, the lattice was initially iterated 300,000 times. The lattice was then further iterated until a measure of statistical stationarity was achieved, up to a maximum of another 500,000 iterations. The quantity which was monitored for stationarity was the mean of the lattice map values at each iteration. The first three statistical moments of both a short- and long-term running series of this quantity were computed. The two series were 75,000 and 300,000 iterations long respectively. For each moment, the short-term and long-term values were compared. If all three pairs of moments were equivalent to within a certain threshold, the lattice was determined to be in a state of statistical stationarity. About a quarter of the runs never achieved this measure of stationarity. Of the 5445 runs resulting in 100-family final states, 1220 failed to achieve stationarity.

Two maps were considered to be in the same family if the cumulative squared difference in map values summed over the 1000 iterations following the run to stationarity was less than 1×10^{-6}.

This method was chosen rather heuristically to see whether lattices with subcritical coupling ($\epsilon < \epsilon_c$) would robustly converge to family-synchronized solutions. The plateaus in Fig. 4, such as the set of 3-family solutions, suggest a perspective which contrasts with that of Kaneko [Kaneko, 1989, Kaneko, 1990], who drew analogies between the phase portraits of

conventional thermodynamics and the final states of a globally-coupled logistic map lattice. In those works, Kaneko used a 200-map lattice with 500 randomly-initialized runs at each point, but with a much smaller time series of iterations. After discarding the first 2000 iterations, he categorized each final state using the next 500. Unfortunately, it appears that such systems can exhibit transients which are much longer than 2500 iterations.

The boundary between one-family and two-family states in Fig. 4 approximately follows the critical coupling threshold (5) for chaotic regimes of the logistic map. However, there are runs which converge to fully-synchronized states at sub-critical coupling values, and regions in which stable solutions with both one and two families appear to fill a significant fraction of phase space volume.

The period-three window around $a \simeq 1.76$ is clearly evident in the appearance of a tongue of fully-synchronized states extending to relatively low coupling values. Note also the "island" of one family states at $\epsilon \simeq 0.15$. This region of map parameter space will be explored in more detail in Section 4.1.

The lines that define the boundaries of a given plateau generally run diagonally across the ϵ-a plane. This is a manifestation of a sort of competition between the synchronizing or stabilizing influence of increased coupling and the destabilizing influence of increased map parameter. In the direction transverse to these boundaries, toward higher map parameter or lower coupling strength, there is a generally smooth increase in the number of families. This trend accelerates rapidly until a sort of "wall" is encountered. At this point, the number of families increases quickly until the limit of full desynchronization is reached. The abrupt changes and the complexity of the results in this region of rapid desynchronization suggest that a more finely-grained exploration of parameter space might help to uncover hidden detail and structure.

4.1 Two-dimensional Sections

A more refined study of the distribution of stationary final states was performed for three representative map parameter values: $a = 1.9$, $a = 1.76$, and $a = 1.5$. For these sections, 200 independent runs with randomly-chosen initial conditions were used, and an empirical attempt was made to distinguish between different solutions. Each stationary state was categorized by the number of families in the solution, and by information about each of its families. Each family time series of 1000 iterations was characterized by its mean, its variance, and its periodicity if it had one.

For most of the parameter space domain explored in this manner, the number of distinct solutions found is nearly as large as the number of initial conditions used. If the methods used to distinguish between solutions work as intended, then this is good evidence of attractor crowding [Weisenfeld and Hadley, 1989]. There is a tendency for there to be fewer unique solutions at higher values of the coupling strength.

The existence of simultaneous stable solutions and the general trend for a greater number of families as the coupling strength is reduced is evident in Fig. 5. It is surprising to see that after the complete desynchronization limit is reached at $\epsilon = 0.04$, there is a window at $\epsilon = 0.01$ in which a host of family-synchronized solutions becomes apparent once more. In this window,

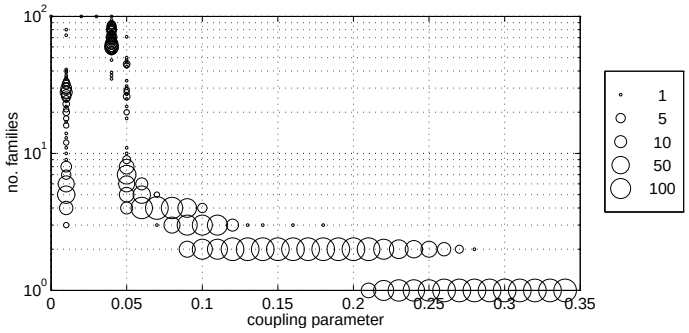

Figure 5: Two-dimensional slice through the parameter space of Fig. 4 at $a = 1.5$. The size of the symbol as given by the key is the number of randomly-initialized runs out of 200 which manifested the given number of families in their stationary final states. For clarity, runs with 100-family results have been portrayed with the smallest symbols.

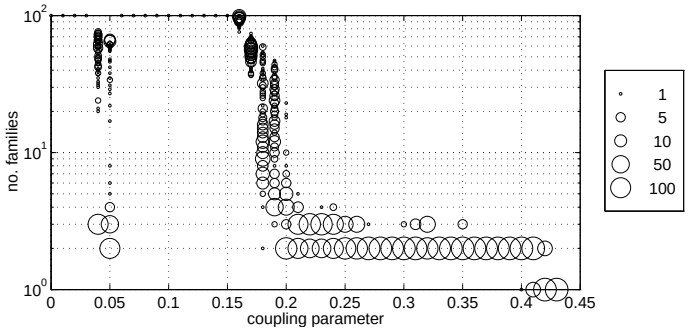

Figure 6: Same as Fig. 5 but at $a = 1.9$.

solutions with 4-7 families and 26-30 families are apparently more prevalent.

The same general features are evident at $a = 1.9$ (Fig. 6). The critical coupling value of 0.4225 [Ding and Yang, 1997] is empirically confirmed here; of the 200 runs at $\epsilon = 0.43$, all had fully-synchronized stationary states. The desynchronization wall occurs near the higher coupling value of $\epsilon = 0.19$, and the window of low-coupling family-synchronized solutions occurs between $\epsilon = 0.04$ and $\epsilon = 0.05$. Once more, there is evidence for a bimodal distribution of number of families in final states in this window, with peaks at around $k = 3$ and $k = 60$. A conjecture concerning the existence of this window at low coupling values will be presented in Sec. 5.

A section through the period-three window (Fig. 7) reveals features which appear to be qualitatively different. As one would expect, at zero coupling only three-family solutions are found. At $\epsilon = 0.01$, there are a few three-family solutions, with the remainder being completely desynchronized. There is a peculiar structure to the desynchronization wall between $\epsilon = 0.13$

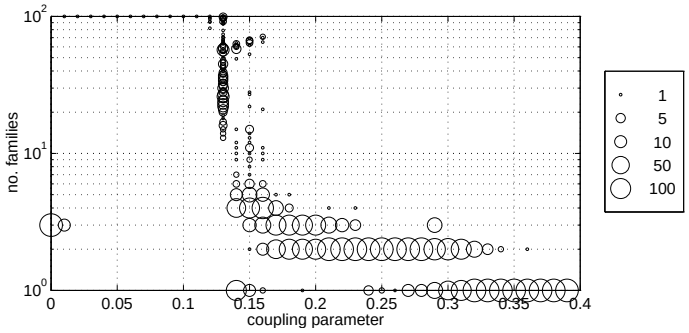

Figure 7: Same as Fig. 6 but at $a = 1.76$. This is in the period-three window of the uncoupled logistic map.

and $\epsilon = 0.16$, in which some preference for 60-70 family solutions is shown. Fully-synchronized solutions persist to much lower coupling strengths, and the "island" of one-family states (Sec. 4 and Fig. 4) is clearly evident. Of the three sections which were analyzed in this fashion, this is the only one for which fully-synchronized solutions coexist with final states having three and more families.

It should be noted that during this study, we never found a solution in which member families had differing periodicities. For instance, if one family was period-12, all members were. If one was chaotic, all families were chaotic.

5 Simplified Dynamics

To develop a better understanding of the dynamics at play here, it is instructive to retreat momentarily from the full complexity of the 100-dimensional lattice of fully chaotic maps. In this section, we discuss the dynamics of much smaller lattices of non-chaotic maps. In particular, we will be dealing with regions of the logistic map in which uncoupled maps fall uniquely onto stable period-two or period-four attractors.

5.1 Period-Two Maps

From about $a = 0.74$ to $a = 1.24$, the uncoupled logistic map manifests a single stable solution, that of a period-two oscillator (Fig. 1). There is also an unstable fixed point at $(-1 + \sqrt{1 + 4a})/2a$. Considering both stable and unstable solutions, there are three periodic points of the map. Bifurcation diagrams can be constructed for a lattice with some given number of maps by considering all the unique possible combinations of solutions as a function of number of periodic points and number of maps. Since position within the lattice is unimportant for globally-coupled systems, we are interested in the number of unique combinations and not the number of permutations. For instance, with the three periodic points coded as X_{high}, X_{fixed}, and X_{low}, there are six unique combinations for a two-map system (Table 1).

Condition	Map 1	Map 2
1	X_{low}	X_{low}
2	X_{low}	X_{fixed}
3	X_{low}	X_{high}
4	X_{fixed}	X_{fixed}
5	X_{fixed}	X_{high}
6	X_{high}	X_{high}

Table 1: Combinations of initial conditions for two-map lattice in the period two window.

Each combination forms an initial condition for the tracing of one branch of a bifurcation diagram. The procedure involves starting just above $\epsilon = 0$ with the maps partitioned according to one combination of the periodic points. Since the coupling strength is non-zero, we expect that the values of the periodic points will have shifted by some small amount. Using Newton's method for zero finding with initial guesses given by the uncoupled periodic points, we determine the actual values of the periodic points for that branch at the given coupling strength. The Jacobian matrix is also computed, and from its eigenvalues we determine whether the particular solution is stable or unstable at that coupling strength. The procedure is continued for an incrementally larger value of ϵ with the just-determined periodic points as the initial guesses.

In Fig. 8(a), we see the results of tracing all six possible branches. The results from both maps in the lattice are plotted. The solid horizontal lines at the top and bottom represent fully-synchronized states, in which both maps are oscillating in phase between the two stable periodic points. The top line corresponds to condition #6 of Table 1 and the bottom line to condition #1. The horizontal dashed line in the center of the plot represents condition #4, the fully-synchronized condition in which both maps are started at the fixed-point. The two stable curving branches represent condition #3, in which one map is initialized at each of the two periodic points. This is an out-of-phase state. As the coupling strength is increased, the maps feel each other to a greater extent and consequently, the periodic points are drawn together. Eventually, this solution becomes unstable. The remaining unstable curving branches represent conditions #2 and #5, for which one map is initialized at the fixed point and the other at one of the two periodic points.

The diagram becomes more involved in Fig. 8(a), for which we have four maps in the lattice and more than twice as many possible combinations of initial conditions. Of the 15 branches traced in this diagram, only 9 are new. There are six combinations which effectively reduce to a two-map lattice. Two more stable branches are generated, depicted by the solid lines terminating at around $\epsilon = 0.12$. These represent the partitioning of one map into one periodic point and three into another. We see already the emergence of multiple stable solutions.

With five maps, an equipartition solution is not possible. The stable out-of-phase solutions shown in Fig. 8(c) are of two sorts: a partitioning of 1:4 into the periodic points, and a 2:3 partitioning. The 1:4 solution becomes unstable at a lower coupling value than the more

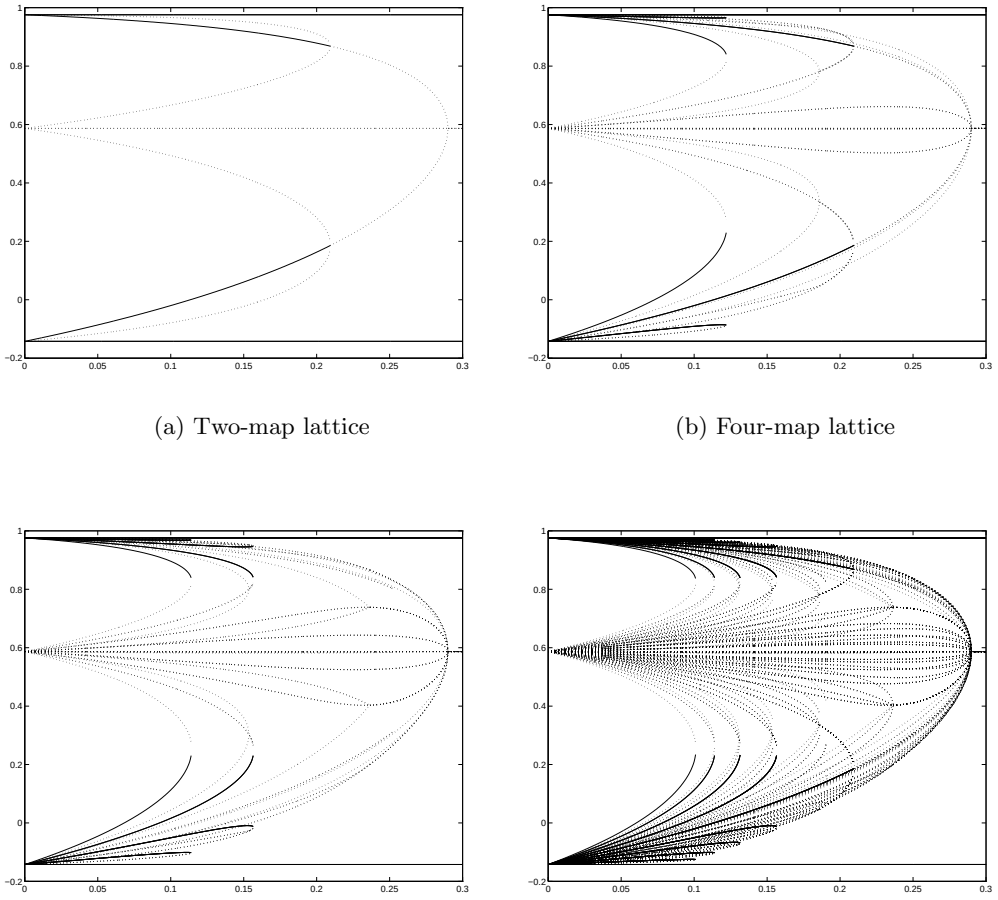

(a) Two-map lattice

(b) Four-map lattice

(c) Five-map lattice

(d) Ten-map lattice

Figure 8: Bifurcation diagrams for lattices of varying size when the map parameter $a = 1.2$ is in the period-two window. Stable solutions are depicted with a solid line, unstable solutions with a dashed line. In all cases, the horizontal axis represents coupling strength ϵ.

balanced 2:3 solution.

Finally with the ten maps of Fig. 8(c) we see one way in which attractor crowding might develop. As the number of maps increases, the number of stable solutions at low ϵ increases.

5.2 Period-Four Maps

Between $a = 1.24$ and $a = 1.36$, the uncoupled logistic map is characterized by a single stable period-four solution (Fig. 1). The fixed point of the map persists as an unstable solution, and

the period-two points are also solutions. This means that there are seven initial conditions in which to partition the maps to find each branch of the bifurcation diagram.

The bifurcation diagrams of Fig. 9 are characterized by a compression and repetition of the period-two map bifurcation diagrams. This additional complexity yields a further set of stable solutions at low coupling strengths.

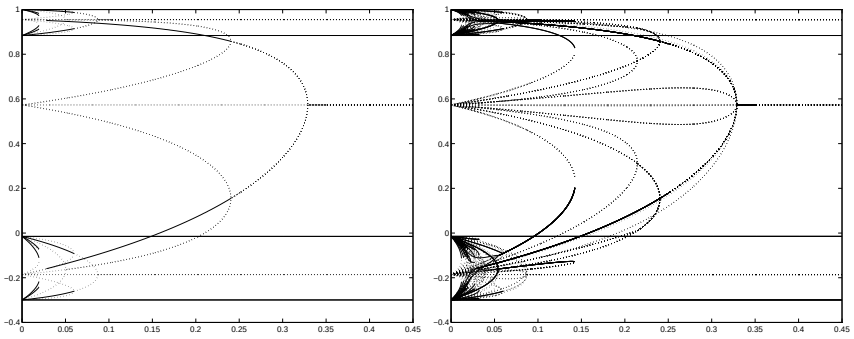

(a) Two-map lattice (b) Four-map lattice

Figure 9: As in Fig. 8, but for map parameter $a = 1.3$ in the period-four window.

6 Stability of Two-Family Solutions

When a lattice assumes a stable family-synchronized solution, its dynamics are vastly simplified. The dynamics of an N-map lattice evolving as k families may simply be written as a k-dimensional map. For instance, let $k = 2$ with families x and y of size N_x and N_y respectively. If we define $N_x/N = \alpha$ and $N_y/N = 1 - \alpha$, then the system evolution at iteration i may be written as

$$\begin{aligned} x_{i+1} &= (1-\epsilon)f(x_i) + \epsilon S_i \\ y_{i+1} &= (1-\epsilon)f(y_i) + \epsilon S_i, \\ &\text{where the mean field is} \\ S_i &= \alpha f(x_i) + (1-\alpha) f(y_i). \end{aligned} \tag{6}$$

This leads to the determination of criteria for the linear stability of a two-family system. A perturbation $\xi(n)$ to each map $x(n)$ and a perturbation $\eta(m)$ to each map $y(m)$ evolve according to

$$
\begin{aligned}
\xi(n)_{i+1} &= (1-\epsilon)f'(x_i)\xi(n)_i + \epsilon\sigma_i \\
\eta(m)_{i+1} &= (1-\epsilon)f'(y_i)\eta(m)_i + \epsilon\sigma_i, \\
&\text{with} \\
\sigma_i &= \alpha f'(x_i)\sum_{n=1}^{N_x}\xi(n)_i + (1-\alpha)f'(y_i)\sum_{m=1}^{N_y}\eta(m)_i.
\end{aligned}
\tag{7}
$$

If all the maps within each family are subject to the same perturbation (i.e., $\xi(n) = \xi$ and $\eta(n) = \eta$), then the problem reduces to that of dynamics within the synchronization manifold. The more intriguing question, however, involves the remaining stability exponents, which are transverse to the synchronization manifold and thus describe the linear stability of the two-family state. If we assume that σ_i is identically zero, then we can search for two cases: either $\sum_{n=1}^{N_x}\xi(n) = 0$ and $\eta(m) = 0$, or $\xi(n) = 0$ and $\sum_{m=1}^{N_x}\eta(m) = 0$. The first case gives

$$\xi(n)_{i+1}/\xi(n)_i = (1-\epsilon)f'(x_i), \tag{8}$$

and the second

$$\eta(m)_{i+1}/\eta(m)_i = (1-\epsilon)f'(y_i). \tag{9}$$

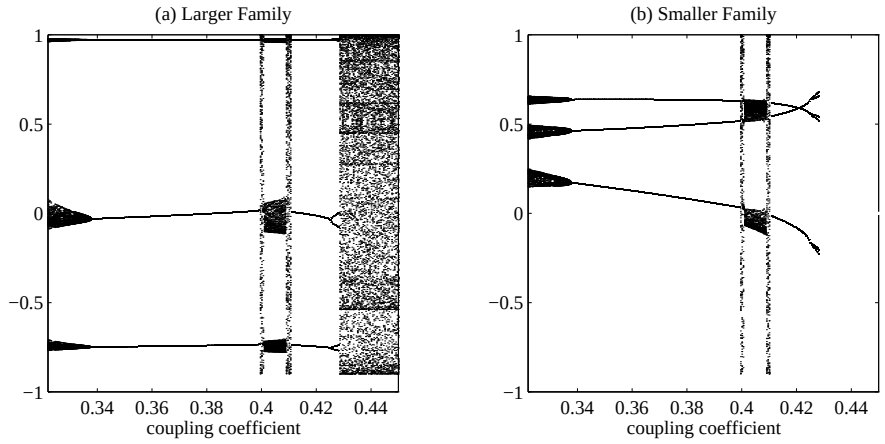

Figure 10: Bifurcation diagram for a particular solution as a function of coupling parameter ϵ. This is a two-family (10 and 90 members) period-three solution generated at $a = 1.9$ and $\epsilon = 0.388$. At each successive value of the coupling parameter, the lattice was initialized with the stationary final state of the lattice from the previous coupling parameter value. (a) Larger family. (b) Smaller family. For $\epsilon > \epsilon_c$ at about 0.4225, the lattice is fully synchronized and only one family exists.

The stable regime of one particular two-family solution is depicted in Fig. 10. The initial solution is period-three. The bifurcation which occurs from $\epsilon = 0.334$ to $\epsilon = 0.321$ is shown in detail in Fig. 11.

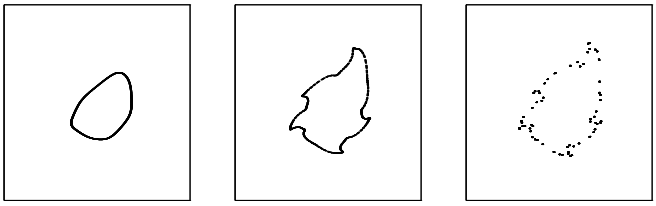

(a) $\epsilon = 0.334$ (b) $\epsilon = 0.33$ (c) $\epsilon = 0.3292$

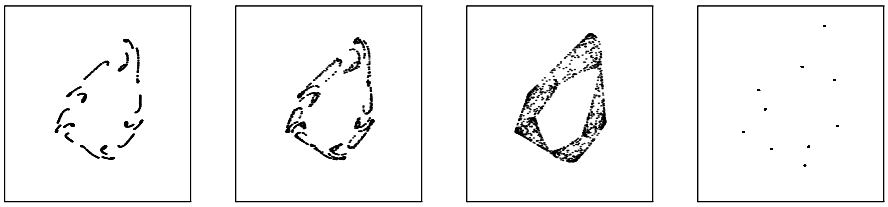

(d) $\epsilon = 0.3286$ (e) $\epsilon = 0.32855$ (f) $\epsilon = 0.328$ (g) $\epsilon = 0.327$

(h) $\epsilon = 0.3268$ (i) $\epsilon = 0.3264$ (j) $\epsilon = 0.321$

Figure 11: Third return map for break up of the two-family solution of Fig. 10. The smaller family third returns are plotted on the horizontal axis and those of the larger family on the vertical. Panels depict succesively smaller coupling strengths. Linear stability is lost at about $\epsilon = 0.322$.

7 Acknowledgements

Antonello Provenzale was responsible for introducing me to a fascinating subject and patiently teaching me the fundamentals needed to explore it. Despite the lack of drinkable espresso in Woods Hole, Antonello was always cheerful and positive. Neil Balmforth kept me hopping

with a constant flux of innovative ideas for exploring the dynamics of our system. I benefited from discussions about related systems with both Mike Shelley and Ed Spiegel. Jean-Luc Thiffeault and Eric Chassignet provided valuable technical assistance. Steve Meacham and Phil Morrison have suggested some interesting directions for future research. Thanks also to George Veronis and all the other softball players for organizing a great summer league.

References

[Ding and Yang, 1997] Ding, M. and Yang, W. (1997). Stability of synchronous chaos and on-off intermittency in coupled map lattices. *Phys. Rev. E*, 56(4):4009–4016.

[Kaneko, 1989] Kaneko, K. (1989). Chaotic but regular posi-nega switch among coded attractors by cluster-size variation. *Phys. Rev. Lett.*, 63(3):219–223.

[Kaneko, 1990] Kaneko, K. (1990). Clustering, coding, switching, hierarchical ordering, and control in a network of chaotic elements. *Physica D*, 41:137–172.

[Ott, 1993] Ott, E. (1993). *Chaos in dynamical systems*. Cambridge University Press, Cambridge, Great Britain.

[Weisenfeld and Hadley, 1989] Weisenfeld, K. and Hadley, P. (1989). Attractor crowding in oscillator arrays. *Phys. Rev. Lett.*, 62(12):1335–1338.